Hindered intermolecular stacking of anti-parallel telomeric G-quadruplexes

Luca Bertini ; Valeria Libera; Sara Catalini ; Giorgio Schirò ; Andrea Orecchini ;
Renzo Campanella ; Valentina Arciuolo ; Bruno Pagano ; Caterina Petrillo ; Cristiano De Michele;
Lucia Comez ; Alessandro Paciaroni
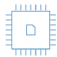
Check for updates

View Online   Export Citation

AIP
Publishing

Hindered intermolecular stacking of anti-parallel telomeric G-quadruplexes

View Online   Export Citation   CrossMark

Luca Bertini,[1] Valeria Libera,[1] Sara Catalini,[1] Giorgio Schirò,[2] Andrea Orecchini,[1] Renzo Campanella,[1] Valentina Arciuolo,[3] Bruno Pagano,[3] Caterina Petrillo,[1] Cristiano De Michele,[4] Lucia Comez,[5,a] and Alessandro Paciaroni[1,a]

AFFILIATIONS

[1] Department of Physics and Geology, University of Perugia, via Alessandro Pascoli, 06123 Perugia, Italy
[2] Univ. Grenoble Alpes, CEA, CNRS, Institut de Biologie Structurale, F-38044 Grenoble, France
[3] Department of Pharmacy, University of Naples Federico II, 80131 Naples, Italy
[4] Department of Physics, University of Rome La Sapienza, 00185 Rome, Italy
[5] CNR-IOM c/o Department of Physics and Geology, University of Perugia, 06123 Perugia, Italy

[a] Authors to whom correspondence should be addressed: comez@iom.cnr.it and alessandro.paciaroni@unipg.it

ABSTRACT

Telomeric G-quadruplexes (G4s) are non-canonical DNA structures composed of TTAGGG repeats. They are extensively studied both as biomolecules key for genome stability and as promising building blocks and functional elements in synthetic biology and nanotechnology. This is why it is extremely important to understand how the interaction between G4s is affected by their topology. We used small-angle x-ray scattering to investigate the end-to-end stacking of antiparallel telomeric G-quadruplexes formed by the sequence $AG_3(T_2AG_3)_3$. To represent the experimental data, we developed a highly efficient coarse-grained fitting tool, which successfully described the samples as an equilibrium mixture of monomeric and dimeric G4 species. Our findings indicate that the antiparallel topology prevents the formation of long multimeric structures under self-crowding conditions, unlike the hybrid/parallel structures formed by the same DNA sequence. This result supports the idea that the stacking of monomeric G-quadruplexes is strongly affected by the presence of diagonal loops.

I. INTRODUCTION

G-Quadruplexes (G4s) represent a unique and fascinating class of non-canonical nucleic acid secondary structures that are prone to form in G-rich DNA/RNA sequences. These structures arise from the stacking of two or more G-quartets, formed by the association of four guanine bases through Hoogsteen hydrogen bonding.[1–4] The nucleotides that are not engaged in the Hoogsteen networks participate in the formation of loops bridging the extremal tetrads. Coordination of a central cation with the O6 atoms of the guanine bases is essential to the stability of the structure. A distinctive feature of G4s is their structural polymorphism, which is embodied in the diversity of their possible conformations depending on the specific nucleotide sequence and the environmental conditions.[5,6] Based on

the relative orientation of the G-tracts in the 5′–3′ direction, G4s can be classified as parallel, antiparallel, and hybrid[3,4] (see Fig. 1). In the parallel topology, all the G-tracts run in the same direction, whereas in the antiparallel topology, two adjacent G-tracts run in opposite directions. The hybrid conformation combines features of both parallel and antiparallel arrangements. Two parallel G-tracts are usually connected by external (or propeller) loops, while two antiparallel G-tracts are connected by lateral loops if they are contiguous and by diagonal loops if they are on the opposite side of the G-quartet.

Putative G4-forming sequences are widespread in the human genome.[7] Nevertheless, their higher concentration in specific locations, such as gene promoters and telomeric regions, suggests their involvement in significant biological processes such as gene
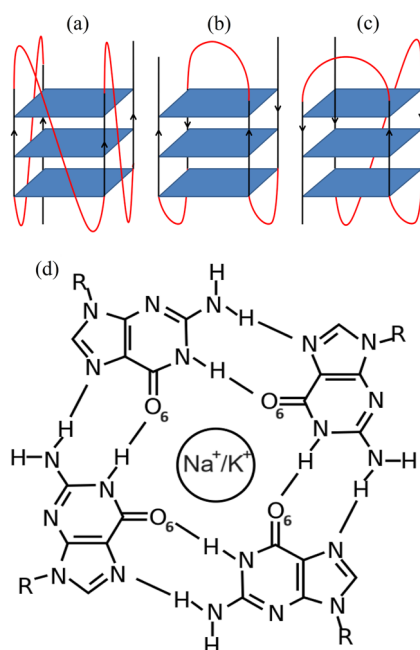
FIG. 1. Schematic representation of parallel (a), antiparallel (b), and hybrid (c) G4 topologies. (d) Chemical representation of the G-tetrad.

expression and telomere maintenance.[1,2,8] Indeed, it was shown that, when G4s are not properly unwound by helicases, issues such as telomeric lagging strand defects and slowed replication through telomeres in combing assays arise.[9] Moreover, the distinctive physico-chemical properties of these structures have led to the development of numerous applications in the fields of materials science and nanotechnology. In particular, the strong dependence of G4 stability and topology on the type and concentration of cations in solution makes them well-suited for use as switchable components in molecular machines and programmable nanostructures.[10,11]

At present, the vast majority of studies on G4 structures are concerned with their monomeric state. Cellular nuclei, however, are highly crowded environments, and putative G4-forming sequences may be located in DNA regions quite close to each other.[12–14] Therefore, the interactions between different G4 sub-units might lead to multimeric higher-order structures under physiological conditions.[15] Even though base-pairing is the most common mechanism leading to the multimerization of nucleic acids, stacking interactions at the level of extremal tetrads are also known to induce the formation of self-assembled G4 aggregates. The length of the resulting higher-order structures might vary from a few G4s (mainly dimers and trimers) to a few hundred G4s in the case of G-wires.[16–19] At the telomeric level, the biological role of multimeric structures has been associated with protein recognition and telomerase processing.[8] In addition, the presence of multimeric G4 structures has been linked with neurological disorders.[20] Furthermore, a deeper understanding of stacking interactions and self-assembly of G4 sub-units could play a crucial role in the fabrication of well-ordered nano-networks.[21] Indeed, well-ordered DNA nano-networks have emerged as promising platforms in nanotechnology

due to their unique structural properties and programmability.[22,23] High-ordered G4s could be designed with precise control over size, shape, and functionality. These networks can offer a versatile framework for various applications, including drug delivery, biosensing, and nanoelectronics.

In a recent study, we have investigated the multimerization of the model human telomeric sequence $AG_3(TTAG_3)_3$ (Tel22) in K^+ solution, as induced by self-crowding.[24] For this purpose, we introduced a novel approach combining Extremely Coarse Grained (ECG) Monte Carlo Simulations and Small Angle X-ray Scattering (SAXS) experiments. Our results showed how stacking interactions at the level of the extremal tetrads lead to the formation of aggregates characterized by an exponential chain length distribution. Furthermore, we observed an increase in the fraction of parallel structures, along with a decrease in the syn-anti and diagonal + lateral loop structural components, upon increasing the average multimer chain length. Here, we report the results of SAXS measurements performed to investigate the effect of self-crowding on the multimerization of Tel22 in Na^+ solution and to further elucidate the subtle interplay between G4 topology and self-assembly induced by stacking interactions. In contrast to the case of Tel22 (K^+), Tel22 (Na^+) is expected to adopt a mainly antiparallel topology.[25,26]

In order to accurately reproduce the obtained SAXS profiles, we developed an ECG fitting tool specifically designed to identify the multimeric geometry that optimally reproduces the SAXS data. We observed that the antiparallel arrangement inhibits the formation of extensive multimeric structures under self-crowding conditions, unlike the hybrid/parallel structures formed by the identical DNA sequence.

II. M TERI LS ND METHODS

. Sample preparation

The lyophilized human telomeric sequence Tel22 was purchased from Eurogentec (Seraing, Belgium) and dissolved in a 50 mM phosphate buffer at pH 7, 0.3 mM EDTA, and 150 mM NaCl. A stock solution with a DNA concentration of C ~ 13 mM was annealed by heating up to 95° and then slowly cooling down to room temperature. The solution was left overnight at room temperature. Subsequently, centrifugation of the solution at 15 °C and 15 000 rpm for 120 s was performed. At this point, three solutions at C = 0.6 mM, C = 1.2 mM, and C = 4.5 mM were prepared from the centrifuged solution. The molarity of the solutions was determined by UV absorption spectroscopy, using a molar extinction coefficient $\varepsilon = 228\,500$ M^{-1} cm^{-1} at 260 nm. Finally, the three solutions were further annealed and left at room temperature overnight. This procedure was employed in our previous work to obtain the formation of aggregates in the case of Tel22 (K^+).[24]

In order to obtain a Tel22 sample in the purest possible monomeric state, a solution with a DNA concentration of C = 1 mM was annealed using the same buffer. Subsequently, Size Exclusion Chromatography (SEC) was performed using an equilibrated Superdex 75 16/600 column kept at a constant flow rate of 0.5 ml/min. The loading concentration and injection volume of the sample were, respectively, C = 1 mM and V = 300 μl. After collecting the monomeric fraction, UV absorption spectroscopy measurements were performed to assess the molarity of the solution, which resulted to be C = 62 μM.

B. S XS experiment

The SAXS experiment was performed at the BM29 beamline at the European Synchrotron Radiation Facility (ESRF) in Grenoble, France. The incident energy was 12.5 keV (incident wavelength 0.099 nm), and the scattering vector range was [0.044–5.21] nm^{-1}. All the patterns were acquired at temperature T = 20 °C, and the buffers were also measured in order to perform a proper subtraction of the solvent contribution to the sample environment.

C. Circular dichroism experiment

Circular Dichroism (CD) measurements of Tel22 (Na$^+$) at concentrations C = 62 μM, C = 0.6 mM, C = 1.2 mM, and C = 4.5 mM and of the Tel22 SEC monomer were performed using a Jasco J-810 spectropolarimeter in 0.01–0.1 mm path length quartz cells. Spectra were collected in the range from 220 to 330 nm with a scan speed of 50 nm/min. All the CD profiles were acquired at room temperature. CD data were expressed as the difference in the molar absorption $\Delta\varepsilon$ [M^{-1} cm^{-1}] of the right- and left-handed circularly polarized light.

D. Polyacrylamide gel electrophoresis (P GE)

Native 20% PAGE gels were prepared with 29:1 acrylamide/bisacrylamide solution and 1× TBE (Tris–Borate–EDTA), pH 7.0. Gels were run at 4 °C and 120 V for 1 h. Oligonucleotide samples annealed at 0.6, 1.2, and 4.5 mM concentrations were diluted to 20 or 50 μM concentration in a 50 mM phosphate buffer at pH 7.0, supplemented with 0.3 mM EDTA and 150 mM NaCl. A solution of glycerol/TBE was added (10% final) to facilitate sample loading into the wells. Bands were visualized by UV shadowing at 254 nm.

E. ECG fitting

For the analysis of the SAXS data presented in this work, we propose a novel ECG fitting tool. The normalized SAXS intensity corresponding to an arrangement of simple geometric sub-units is reproduced in a computational cost-effective manner. This is achieved by randomly generating N scattering points with uniform number density within the geometric sub-units.[24,27] A histogram containing the distribution of the distances between all possible pairs of points, which corresponds to the pair distance distribution $p(r)$, is then generated, and the normalized form factor is calculated as

$$P_{\text{norm}}(Q) = \frac{\sum_{i=1}^{N_{bins}} p(r_i) \sin(Qr_i)/(Qr_i)}{\sum_{i=1}^{N_{bins}} p(r_i)}, \tag{1}$$

where N_{bins} is the number of bins in the $p(r)$ histogram, r_i is the ith entry, and Q is the momentum transfer.[28] Our algorithm is currently limited to hard cylinder (HC) sub-units but, in principle, could be extended to other geometrical shapes. The various HC sub-units used to construct the fitting model can be translated and rotated with respect to each other to obtain any arbitrary configuration in the three-dimensional space. Subsequently, we implemented a Levenberg–Marquardt algorithm for nonlinear least squares curve-fitting that allows us to identify the HC geometric configuration that best reproduces the experimental SAXS intensity.[29]

F. Fitting models

The SAXS signals of the samples at C = 0.6 mM and C = 1.2 mM concentrations were fitted using a model consisting of a monomer–dimer mixture. The dimer, which is composed of two HCs with radius R and length L, is obtained by aligning the two sub-units on top of each other at distance d = 0.5R between the centers of the extremal bases and then rotating the top HC so that the two central axes form a tilting angle α. A cartoon representation of the model is reported in Figs. 4(a)–4(c). By denoting the contributions of the monomeric and dimeric form factors, respectively, with $P_{mon}^{\text{norm}}(Q)$ and $P_{\text{dim}}^{\text{norm}}(Q)$, the overall SAXS intensity can be expressed as

$$I(Q) = CN_A(\Delta\rho)^2 V_{mon}^2 \left[f_{mon}P_{mon}^{\text{norm}}(Q) + 2(1 \quad f_{mon})P_{\text{dim}}^{\text{norm}}(Q) \right], \tag{2}$$

where N_A is Avogadro's number, $\Delta\rho$ is the scattering length density contrast, V_{mon} is the monomer's volume, and f_{mon} is the fraction of HCs in the monomeric state. The radius R and height L of the HCs, which are supposed to be the same in monomers and dimers, were used as fitting parameters along with f_{mon}.

At the highest investigated concentration (C = 4.5 mM), repulsive interactions between the scattering particles were observed. Therefore, Eq. (2) was modified to take into account inter-particle correlations. This can be done by introducing partial static structure factors describing monomer–monomer, monomer–dimer, and dimer–dimer interactions. The present analysis, however, revealed that only a small fraction (namely less than 5%) of the G4 sub-units is involved in the formation of dimers, thus leading to negligible deviations from unity for the monomer–dimer and dimer–dimer partial structure factors.[30] As a consequence, only monomer–monomer interactions were taken into account and the SAXS intensity of the C = 4.5 mM sample was modeled as follows:

$$I(Q) = CN_A(\Delta\rho)^2 V_{mon}^2 \left[f_{mon}S(Q;phi,D)P_{mon}^{\text{norm}}(Q) \right.$$
$$\left. + 2(1 \quad f_{mon})P_{\text{dim}}^{\text{norm}}(Q) \right], \tag{3}$$

where $S(Q; \phi, D)$ is a *corrected* structure factor that is usually employed in the case of non-spherically symmetric scattering particles.[31] By denoting the orientational average of the scattering amplitude of a HC as $\langle f(Q)\rangle$, $S(Q; \phi, D)$ takes the following form:

$$S(Q;\phi,D) = 1 + \frac{|\langle f(Q)\rangle|^2}{I_{mon}(Q)}(S_{PY}(Q;\phi,D) \quad 1). \tag{4}$$

The expression for the monomer–monomer structure factor $S_{PY}(Q; \phi, D)$, which was used in the present work, is that of the hard sphere repulsive potential.[32] ϕ denotes the particles' volume fraction in the solution, and D is the hard sphere diameter.

III. RESULTS ND DISCUSSION

As already observed in the literature, the secondary structures of Tel22 (Na$^+$) and Tel22 (K$^+$) in diluted solutions are quite different, being prevalently antiparallel and hybrid, respectively (see Fig. S1a).[25,33–35] The different behavior of the Tel22 sequence in the
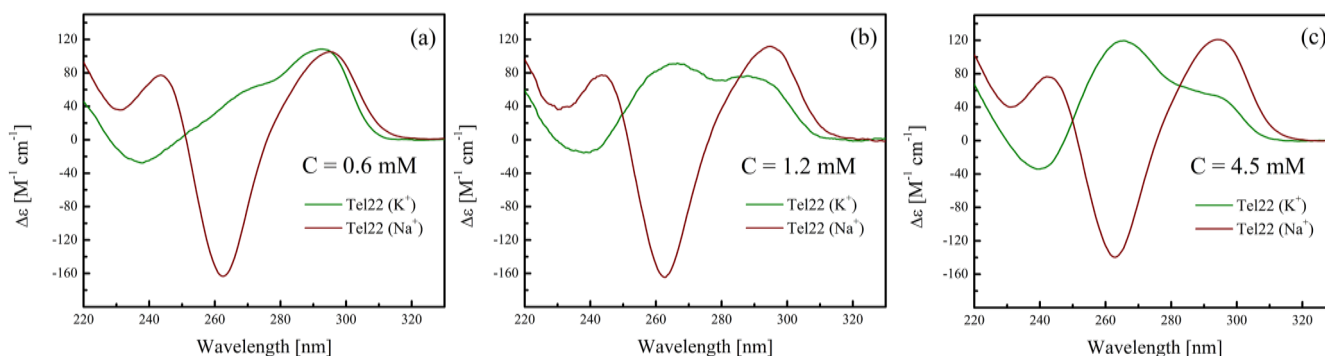
FIG. 2. Comparison between the CD spectra of Tel22 in K⁺ (green) and Na⁺ (brown) solutions at (a) C = 0.6 mM, (b) C = 1.2 mM, and (c) C = 4.5 mM concentrations.

presence of the two cations is even more evident when the DNA concentration is increased, as shown in the CD spectra reported in Fig. 2. In the case of Tel22 (Na^+), the distinctive markers of the antiparallel topology, i.e., a maximum at $\simeq$295 nm and a minimum at $\simeq$260 nm,[36] can be identified for all the samples. The intensity of both these features only displays slight changes with increasing concentration; therefore, no major conformational differences among the samples can be inferred. This finding is in contrast to the case of Tel22 (K^+), where a clear shift from the hybrid toward the parallel topology was observed as a function of concentration, as witnessed by the fact that the shoulder at 265 nm becomes the dominant peak with respect to the maximum at 290 nm.[24]

One can wonder whether the observed topological differences of Tel22 in the two ionic environments are related to the multimerization properties of the involved G4s. SAXS is a particularly suitable technique to answer this question, as it is able to probe the structural properties of biomolecules in the nanometer scale.

In Fig. S1b, a comparison between the SAXS signals of the Tel22 (Na^+) and Tel22 (K^+)[24] monomers is reported. Remarkably, the signals superimpose quite well onto each other, suggesting that the G4 monomeric units in the two ionic environments have

approximately the same dimensions within the experimentally accessible space resolution. This result highlights the difficulty of distinguishing the different topologies of G4s with SAXS. As shown in Fig. S2, the experimental data are reproduced very well for Tel22 (Na^+) by a Hard Cylinder (HC) form factor with the corresponding values for the radius R_{mon} = 1.02 ± 0.02 nm and for the height L_{mon} = 3.1 ± 0.3 nm. These values are very similar to those found for Tel22 (K^+). It is worth noting that, using the HC shape is equivalent to describe the G4 monomer as a homogeneous biomolecule. Actually, in the past, the G4 SAXS form factor has been accurately approximated with a core–shell cylinder model, with an inner core representing the cavity containing the central cations and an outer shell describing guanines, hydrated sugar, and phosphate groups.[37] We verified that this model provides an equivalent reduced chi-squared value as the HC model when fitting the SAXS data of G4 monomers. For this reason, to maintain the ECG fitting method as efficient as possible, we adopted the latter, which employs a lower number of parameters.

As for the samples annealed at high DNA concentrations, the corresponding SAXS intensities are reported in Fig. 3 for both ionic environments at C = 0.6 mM [panel (a)], C = 1.2 mM [panel (b)], and
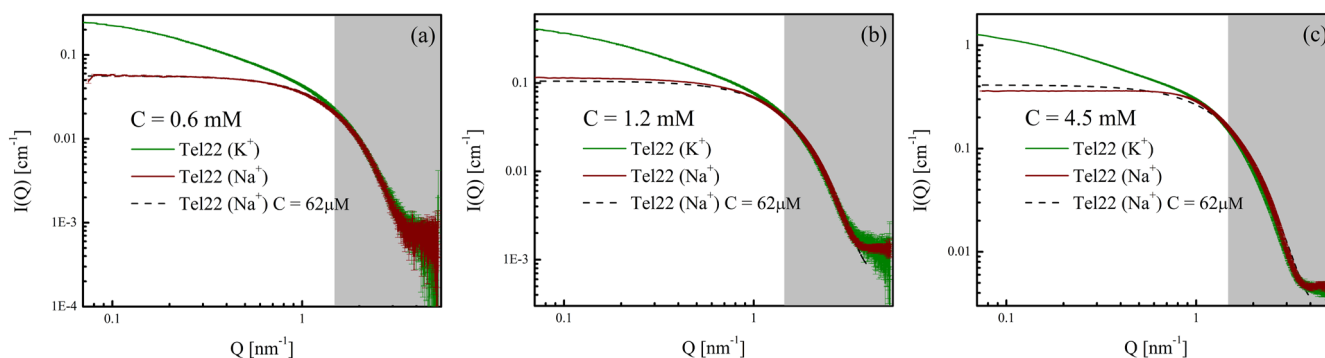
FIG. 3. Comparison between the SAXS curves of Tel22 (K^+) (green) and Tel22 (Na^+) (brown) solutions at (a) C = 0.6 mM, (b) C = 1.2 mM, and (c) C = 4.5 mM. The SAXS curve of Tel22 (Na^+) at C = 62 μM (black dashed line) is also reported to highlight any significant deviation from the monomeric state. The curves of Tel22 (K^+) and Tel22 (Na^+) C = 62 μM have been rescaled by an arbitrary factor to better emphasize the differences in shape with Tel22 (Na^+). The gray area highlights the high-Q region, where all the curves overlap with each other.

C = 4.5 mM [panel (c)]. The quite good overlap of the curves in the high-Q region (gray areas in Fig. 3) once more suggests that the overall shape of the G4 sub-units is similar in the two ionic environments at all the investigated concentrations. In the low-Q region, however, striking differences can be noticed. In Tel22 (K^+), there is an observable excess of scattering over the monomeric plateau, whereas this phenomenon is absent in Tel22 (Na^+). These differences indicate that the formation of exponentially distributed aggregates observed in the K^+ solution does not occur in the presence of Na^+. In light of the CD results, the current findings support the hypothesis according to which antiparallel G4s possess a loop geometry potentially leading to hindered stacking interactions between extremal tetrads.[38]

To provide a quantitative interpretation of the SAXS data, we developed an ECG fitting tool capable of incorporating contributions from multiple HC sub-units (see Sec. II). The SAXS profiles of Tel22 (Na^+) at C = 0.6 mM and C = 1.2 mM concentrations were successfully reproduced using a model comprising a mixture of HC monomers and dimers [see Eq. (2)], thus suggesting a weak level of self-assembly. To improve the stability of the fitting procedure, we set the radius R and length L for the HC sub-units of dimers equal to those of the corresponding monomers. In addition, the tilting angle α formed between the central axes of the two HCs in the dimer was set to be equal to $20°$, according to the results from our previous work on Tel22 (K^+).[24]

Meanwhile, the Tel22 (Na^+) sample at C = 4.5 mM concentration deserves particular attention. A careful examination of the SAXS curve [Fig. 3(c)] reveals a slight drop of the scattered intensity below the monomeric plateau in the low-Q region. This behavior, which has already been observed in both proteins and nucleic acids, is related to the presence of repulsive interactions between the scattering particles.[39–41] The corrected structure factor $S(Q; \phi, D)$ can be approximately retrieved by dividing the SAXS intensity by the Tel22 monomeric form factor [see Eq. (3)] due to the fact that the dimeric species is present for less than 5%. As shown in Fig. S3, we successfully described the corrected structure factor by using the analytical expression $S_{PY}(Q; \phi, D)$ for the Percus–Yevick approximation in the case of the hard sphere potential.[39] The excellent agreement between $S(Q; \phi, D)$ and $S_{PY}(Q; \phi, D)$ is attributed to the fact that the ratio $|\langle f(Q) \rangle|^2 / I_{mon}(Q)$ is very close to 1 for Q values below 1.5 nm^{-1}.

Therefore, we directly analyzed the SAXS curve of Tel22 (Na^+) at C = 4.5 mM concentration by multiplying the scattering intensity of the monomer–dimer mixture by $S_{PY}(Q; \phi, D)$, as in Eq. (3). The cartoon representations of the model for the samples at, respectively, C = 0.6 mM, C = 1.2 mM, and C = 4.5 mM concentrations are shown in Figs. 4(a)–4(c), respectively, along with the SAXS curves and the best fits using Eqs. (2) and (3).

The values of R, L, and f_{mon} resulting from the fits are reported in Table I. The G4 monomeric sub-units are found to have approximately the same dimensions for all the measured samples. The minor changes in these structural parameters are consistent with the small differences at the level of the secondary structure revealed by CD measurements (Fig. 2). Meanwhile, the fraction of dimers f_{dim} slightly increases (from 2.0% to 4.0%) with concentration. The prevalent presence of monomers in all the Tel22 (Na^+) samples was also verified by PAGE measurements. In Fig. S4, we show that at all the concentrations, only one band, corresponding to the monomer
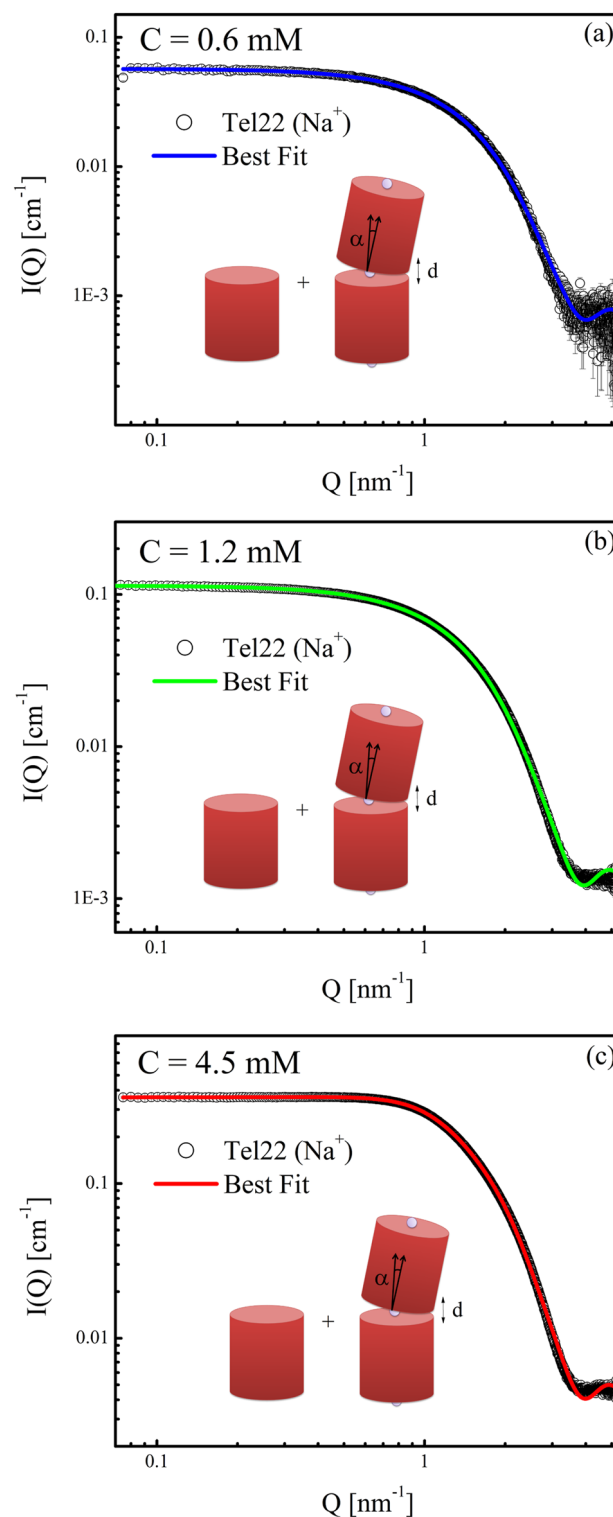
FIG. 4. SAXS curves of Tel22 (Na) at (a) C = 0.6 mM, (b) C = 1.2 mM, and (c) C = 4.5 mM concentrations, along with the corresponding best ECG fits represented, respectively, by blue, green, and red lines. Sketches representing the fitting model are also reported.

TABLE I. Parameters extracted from the ECG fits. The angle α between the central axes of the two HCs in the dimer was fixed to 20° and $f_{dim} = 1$ f_{mon}.

C (mM)	R (nm)	L (nm)	f_{mon} (%)	f_{dim} (%)
0.6	1.04 ± 0.01	3.18 ± 0.05	98.0 ± 0.5	2.0 ± 0.5
1.2	1.03 ± 0.01	3.29 ± 0.01	96.8 ± 0.5	3.2 ± 0.5
4.5	1.06 ± 0.01	3.22 ± 0.01	96.0 ± 0.3	4.0 ± 0.3

species, is clearly visible. This result further highlights the difference with the case of the Tel22 (K$^+$) system, where the average number of stacked units was found to lie in the range 1.94–3.31.[24] The importance of a hybrid/parallel topology to promote multimerization is also supported by the fact that the difference in CD spectra between the 4.5 mM sample and the Tel22 (Na$^+$) monomer, which is related to the dimeric fraction, turns out to be consistent with a hybrid-like fold (see Fig. S5). As for Tel22 (Na$^+$) at C = 4.5 mM, the particle volume fraction ϕ and the hard sphere diameter D associated with the structure factor $S_{PY}(Q; \phi, D)$ were also determined. From the fitting procedure, we obtained the values D = 5.61 ± 0.04 nm and ϕ = 3.90 ± 0.02%, the latter being in agreement with the molar concentration of the sample (see Sec. II of the supplementary material).

The above-mentioned results can be interpreted in light of some insights. The assembly process of G4 monomers is governed by the delicate balance between the repulsive electrostatic interaction resulting from the negative charge of phosphate groups in their backbone and the presence of counterions, which can effectively screen these Coulombic forces. In addition, DNA concentration plays a significant role, as the trade-off between screening distances and inter-particle separation will determine whether repulsive, attractive, or no interactions occur.[41] In the present case, the counterion concentration, and hence the ionic strength of the buffer, is relatively high; thus, an efficient screening of the backbone charges is expected. Nevertheless, SAXS studies on the end-to-end attraction between short DNA suggest that the presence of T loops impeding stacking interactions leads to the persistence of repulsive forces up to high ionic strengths.[40,42] This observation, combined with the CD results, suggests that the peculiar loop geometry of the antiparallel topology (namely, the presence of diagonal loops) discourages stacking attraction but also results in non-negligible repulsive interactions at high DNA concentrations. Therefore, given the weak attractive monomer–monomer interaction witnessed by the small amount of the dimeric fraction, one can speculate that excluded volume effects could be the main source of the observed inter-particle repulsion, consistent with the hard sphere potential approximation.[39]

IV. CONCLUSIONS

Our results show that the self-assembly through stacking interactions of antiparallel G4s formed by the Tel22 sequence in Na$^+$ solution is hindered up to millimolar DNA concentrations. By analyzing the SAXS profiles of the investigated samples using our ECG fitting tool, we found that only a small fraction of G4 dimers is formed under the investigated conditions, with repulsive interactions further limiting aggregation at higher concentrations. In contrast, our previous work demonstrated that the parallel/hybrid topologies are able to promote the formation of Tel22 aggregates under the same self-crowding conditions.[24] The present findings provide valuable insights into the self-assembly of short segments of telomeric sequences, as modulated by topology, ionic strength, and DNA concentration. This kind of knowledge may profoundly impact the design of nanometric devices and scaffolds using DNA G4 as building blocks.

SUPPLEMENTARY MATERIAL

The supplementary material contains the comparison of SAXS monomers, Tel22 (Na$^+$) at C = 4.5 mM, PAGE, estimate of the CD component of the dimeric fraction, and summary of the fitting parameters.

AUTHOR DECLARATIONS

Conflict of Interest

The authors have no conflicts to disclose.

Author Contributions

Luca Bertini: Data curation (equal); Investigation (equal); Writing – original draft (equal). **Valeria Libera**: Investigation (supporting); Writing – original draft (supporting). **Sara Catalini**: Investigation (supporting); Writing – review & editing (equal). **Giorgio Schirò**: Investigation (supporting); Writing – review & editing (equal). **Andrea Orecchini**: Writing – review & editing (equal). **Renzo Campanella**: Writing – review & editing (equal). **Valentina Arciuolo**: Investigation (equal); Writing – review & editing (equal). **Bruno Pagano**: Investigation (equal); Writing – review & editing (equal). **Caterina Petrillo**: Funding acquisition (equal); Writing – review & editing (equal). **Cristiano De Michele**: Investigation (equal); Writing – review & editing (equal). **Lucia Comez**: Investigation (equal); Supervision (equal); Writing – review & editing (equal). **Alessandro Paciaroni**: Conceptualization (equal); Funding acquisition (lead); Investigation (lead); Methodology (equal); Writing – original draft (equal); Writing – review & editing (lead).

DATA AVAILABILITY

The data that support the findings of this study are available within the article and its supplementary material.

REFERENCES

[1] S. Neidle, "Quadruplex nucleic acids as targets for anticancer therapeutics," Nat. Rev. Chem **1**, 0041 (2017).

[2] G. W. Collie and G. N. Parkinson, "The application of DNA and RNA G-quadruplexes to therapeutic medicines," Chem. Soc. Rev. **40**, 5867–5892 (2011).

[3] A. T. Phan, "Human telomeric G-quadruplex: Structures of DNA and RNA sequences," FEBS J. **277**, 1107–1117 (2010).

[4] S. Burge, G. N. Parkinson, P. Hazel, A. K. Todd, and S. Neidle, "Quadruplex DNA: Sequence, topology and structure," Nucleic Acids Res. **34**, 5402–5415 (2006).

[5] V. Libera, F. Bianchi, B. Rossi, F. D'Amico, C. Masciovecchio, C. Petrillo, F. Sacchetti, A. Paciaroni, and L. Comez, "Solvent vibrations as a proxy of the telomere G-quadruplex rearrangements across thermal unfolding," Int. J. Mol. Sci. **23**, 5123 (2022).

[6] J. Kypr, I. Kejnovská, D. Renčiuk, and M. Vorlíčková, "Circular dichroism and conformational polymorphism of dna," Nucleic Acids Res. **37**, 1713–1725 (2009).

[7] V. S. Chambers, G. Marsico, J. M. Boutell, M. Di Antonio, G. P. Smith, and S. Balasubramanian, "High-throughput sequencing of DNA G-quadruplex structures in the human genome," Nat. Biotechnol. **33**, 877–881 (2015).

[8] D. Rhodes and H. J. Lipps, "G-quadruplexes and their regulatory roles in biology," Nucleic Acids Res. **43**, 8627–8637 (2015).

[9] T. M. Bryan, "G-quadruplexes at telomeres: Friend or foe?," Molecules **25**, 3686 (2020).

[10] J.-L. Mergny and D. Sen, "DNA quadruple helices in nanotechnology," Chem. Rev. **119**, 6290–6325 (2019).

[11] J. Dong, M. P. O'Hagan, and I. Willner, "Switchable and dynamic G-quadruplexes and their applications," Chem. Soc. Rev. **51**, 7631 (2022).

[12] J. L. Huppert and S. Balasubramanian, "Prevalence of quadruplexes in the human genome," Nucleic Acids Res. **33**, 2908–2916 (2005).

[13] R. Hänsel-Hertsch, M. Di Antonio, and S. Balasubramanian, "DNA G-quadruplexes in the human genome: Detection, functions and therapeutic potential," Nat. Rev. Mol. Cell Biol. **18**, 279–284 (2017).

[14] D. Komůrková, A. Svobodová Kovaříková, and E. Bártová, "G-quadruplex structures colocalize with transcription factories and nuclear speckles surrounded by acetylated and dimethylated histones H3," Int. J. Mol. Sci. **22**, 1995 (2021).

[15] I. Frasson, V. Pirota, S. N. Richter, and F. Doria, "Multimeric G-quadruplexes: A review on their biological roles and targeting," Int. J. Biol. Macromol. **204**, 89–102 (2022).

[16] T. C. Marsh and E. Henderson, "G-Wires: Self-assembly of a telomeric oligonucleotide, d(GGGGTTGGGG), into large superstructures," Biochemistry **33**, 10718–10724 (1994).

[17] Y. Krishnan-Ghosh, D. Liu, and S. Balasubramanian, "Formation of an interlocked quadruplex dimer by d(GGGT)," J. Am. Chem. Soc. **126**, 11009–11016 (2004).

[18] J.-L. Mergny, A. De Cian, S. Amrane, and M. W. da Silva, "Kinetics of double-chain reversals bridging contiguous quartets in tetramolecular quadruplexes," Nucleic Acids Res. **34**, 2386–2397 (2006).

[19] F. Rosu, V. Gabelica, H. Poncelet, and E. De Pauw, "Tetramolecular G-quadruplex formation pathways studied by electrospray mass spectrometry," Nucleic Acids Res. **38**, 5217–5225 (2010).

[20] E. G. Conlon and J. L. Manley, "Rna-binding proteins in neurodegeneration: Mechanisms in aggregate," Genes Dev. **31**, 1509–1528 (2017).

[21] Q. Wu, S. Liao, G. Yu, J. Wu, and W. Mei, "High-order self-assembly of G-quadruplex DNA: Nano-network formation under the guidance of arene ruthenium(II) complexes," J. Inorg. Biochem. **189**, 81–90 (2018).

[22] L. Stefan and D. Monchaud, "Applications of guanine quartets in nanotechnology and chemical biology," Nat. Rev. Chem **3**, 650–668 (2019).

[23] A. Sondermann, C. Holste, R. Möller, and W. Fritzsche, "Assembly of G-quartet based DNA superstructures (G-Wires)," AIP Conf. Proc. **640**, 93–98 (2002).

[24] B. P. Rosi, V. Libera, L. Bertini, A. Orecchini, S. Corezzi, G. Schirò, P. Pernot, R. Biehl, C. Petrillo, L. Comez et al., "Stacking interactions and flexibility of human telomeric multimers," J. Am. Chem. Soc. **145**, 16166–16175 (2023).

[25] Y. Wang and D. J. Patel, "Solution structure of the human telomeric repeat d[AG3(T2AG3)3] G-tetraplex," Structure **1**, 263–282 (1993).

[26] D. Renčiuk, I. Kejnovská, P. Školáková, K. Bednářová, J. Motlová, and M. Vorlíčková, "Arrangements of human telomere DNA quadruplex in physiologically relevant K solutions," Nucleic Acids Res. **37**, 6625–6634 (2009).

[27] A. Pal, C. A. De Filippo, T. Ito, M. A. Kamal, A. V. Petukhov, C. De Michele, and P. Schurtenberger, "Shape matters in magnetic-field-assisted assembly of prolate colloids," ACS Nano **16**, 2558–2568 (2022).

[28] A. H. Larsen et al., "Shape2SAS: a web application to simulate small-angle scattering data and pair distance distributions from user-defined shapes," J. Appl. Crystallogr. **56**(4), 1287–1294 (2023).

[29] H. P. Gavin, *The Levenberg-Marquardt Algorithm for Nonlinear Least Squares Curve-Fitting Problems* (Department of Civil and Environmental Engineering, Duke University, 2019), Vol. 19.

[30] F. Spinozzi, G. Ceccone, P. Moretti, G. Campanella, C. Ferrero, S. Combet, I. Ojea-Jimenez, and P. Ghigna, "Structural and thermodynamic properties of nanoparticle–protein complexes: A combined saxs and sans study," Langmuir **33**, 2248–2256 (2017).

[31] M. Kotlarchyk and S.-H. Chen, "Analysis of small angle neutron scattering spectra from polydisperse interacting colloids," J. Chem. Phys. **79**, 2461–2469 (1983).

[32] B. Hammouda, *Probing Nanoscale Structures-The Sans Toolbox* (National Institute of Standards and Technology, 2008), pp. 1–717.

[33] B. A. Tucker, J. S. Hudson, L. Ding, E. Lewis, R. D. Sheardy, E. Kharlampieva, and D. Graves, "Stability of the Na form of the human telomeric G-quadruplex: Role of adenines in stabilizing G-quadruplex structure," ACS Omega **3**, 844–855 (2018).

[34] A. Ambrus, D. Chen, J. Dai, T. Bialis, R. A. Jones, and D. Yang, "Human telomeric sequence forms a hybrid-type intramolecular G-quadruplex structure with mixed parallel/antiparallel strands in potassium solution," Nucleic Acids Res. **34**, 2723–2735 (2006).

[35] J. Dai, C. Punchihewa, A. Ambrus, D. Chen, R. A. Jones, and D. Yang, "Structure of the intramolecular human telomeric G-quadruplex in potassium solution: A novel adenine triple formation," Nucleic Acids Res. **35**, 2440–2450 (2007).

[36] R. del Villar-Guerra, J. O. Trent, and J. B. Chaires, "G-quadruplex secondary structure obtained from circular dichroism spectroscopy," Angew. Chem. **130**, 7289–7293 (2018).

[37] P. Mariani, F. Spinozzi, F. Federiconi, H. Amenitsch, L. Spindler, and I. Drevensek-Olenik, "Small angle x-ray scattering analysis of deoxyguanosine 5-monophosphate self-assembing in solution: Nucleation and growth of G-quadruplexes," J. Phys. Chem. B **113**, 7934–7944 (2009).

[38] N. Smargiasso, F. Rosu, W. Hsia, P. Colson, E. S. Baker, M. T. Bowers, E. De Pauw, and V. Gabelica, "G-Quadruplex DNA assemblies: Loop length, cation identity, and multimer formation," J. Am. Chem. Soc. **130**, 10208–10216 (2008).

[39] F. Zhang, M. W. Skoda, R. M. Jacobs, R. A. Martin, C. M. Martin, and F. Schreiber, "Protein interactions studied by SAXS: Effect of ionic strength and protein concentration for BSA in aqueous solutions," J. Phys. Chem. B **111**, 251–259 (2007).

[40] L. Pollack, "Saxs studies of ion–nucleic acid interactions," Annu. Rev. Biophys. **40**, 225–242 (2011).

[41] Y. Chen and L. Pollack, "SAXS studies of RNA: Structures, dynamics, and interactions with partners," WIREs RNA **7**, 512–526 (2016).

[42] L. Li, S. A. Pabit, J. S. Lamb, H. Y. Park, and L. Pollack, "Closing the lid on DNA end-to-end stacking interactions," Appl. Phys. Lett. **92**, 223901 (2008).

11 September 2024 06:52:18